THE JOURNAL OF PHYSICAL CHEMISTRY C
A JOURNAL OF THE AMERICAN CHEMICAL SOCIETY

pubs.acs.org/JPCC

Article

High Pressure Polymerization of 2,6-Diethynylpyridine

Yunfan Fei, Yapei Li, Puyi Lang, Xingyu Tang, Peijie Zhang, Guangwei Che, Xiao Dong, Kuo Li,* and Haiyan Zheng*

Cite This: *J. Phys. Chem. C* 2024, 128, 7286−7293

Read Online

ACCESS | Metrics & More | Article Recommendations | Supporting Information

ABSTRACT: Pressure induced polymerization (PIP) of unsaturated molecules like aromatics is highly focused on its production of novel carbon materials like diamond nanothread and graphane. However, the high stability of the aromatic molecules results in a high polymerization pressure at room temperature. To reduce the reaction pressure of the aromatic ring, here we introduced conjugated alkynyl, investigated the PIP of 2,6-diethynylpyridine (2,6-DEP) up to 30.7 GPa, and successfully obtained one-dimensional (1-D) ordered polymers below 10 GPa. In situ Raman and IR spectra show that the alkynyl starts to react at 4−5 GPa. At 5.4 GPa, the critical crystal structure of 2,6-DEP was investigated by in situ X-ray diffraction, and the shortest intermolecular distance was determined as 2.90 Å, between the pyridine ring. The product recovered from 10 GPa shows clearly a 1-D structure via transmission electron microscopy (TEM), and strong diffractions at d = 7.5 and 5.2 Å, corresponding to the interplane distance of the stacked 1-D polymer. Theoretical simulations show that the reaction starts between the alkynyl groups, after which the aromatic rings are drawn close to each other and react. Combining the predicted reaction and the experimental result, we concluded possible models of the product. Our study shows that alkynyl is a good initiator for reducing the polymerization pressure of the aromatics and therefore allows the synthesis of ordered 1-D carbon materials in large scale.

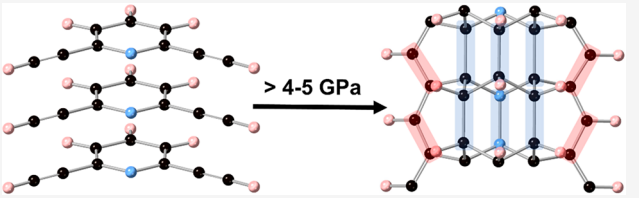

INTRODUCTION

Pressure-induced polymerization (PIP) is a powerful method to synthesize novel diamond-based materials from organic molecules.[1] Among the numerous unsaturated organics, aromatic molecules were widely studied because their columnar $\pi\cdots\pi$ packing facilitates the intermolecular bonding and therefore the formation of diamond nanothreads (DNThs) and related sp^3-C materials. For example, many DNThs and graphane materials were synthesized by compressing benzene,[2] pyridine,[3] furan,[4] pyridazine,[5] *s*-triazine,[6] aniline,[7] and benzene-hexafluorobenzene cocrystal[8] as well as other aromatic molecules. However, the reaction pressure of most aromatics at room temperature is above 10 GPa, typically at 20 GPa, and large-scale preparation is therefore very difficult. In contrast, alkynes generally have a higher reactivity and lower reaction pressure thresholds at room temperature. Acetylene polymerizes around 4 GPa at room temperature and form graphane at higher pressure.[9−12] This reminds us that the introduction of alkynyl into the benzene ring may reduce the reaction pressure of the benzene ring.

According to the literature, as the simplest molecule involving both the alkynyl and the aromatic ring, phenylacetylene (PA) reacted above 8 GPa to form poly(phenylacetylene) chains; that is, only the alkynyls reacted with each other.[13] The benzene ring of 1,4-diethynylbenzene (DEB) polymerized above 10 GPa to form an ordered sp^3-carbon nanothread-type structure via cycloaddition along the stacking axis, while some alkynyls may react along the nanothread backbone.[14] Diphenylacetylene (DPhA) was reported to react at 25−30 GPa to produce "double core" DNThs with the two cores bound by a *cis*-polyacetylene-like backbone. The benzene ring and alkynyl are polymerized into nanothread and *cis*-polyacetylene, respectively.[15] These reports did not show the positive effect of alkynyl on the reaction pressure of benzene. However, recently we found that 1,4-diphenylbutadiyne (DPB) polymerized via [4 + 2] dehydro-Diels−Alder (DDA) reaction between phenyl and phenylethynyl at 10 GPa and produced crystalline graphitic nanoribbon.[16] The DDA reaction is a concerted reaction involving alkynyl and phenyl, instead of independent reactions of alkynyl and phenyl. 1,3,5-Triethynylbenzene (TEB) also polymerized via DDA reaction between ethynylphenyl and phenyl at 4 GPa and formed a one-dimensional (1-D) sp^2−sp^3 carbon nanoribbon,[17] which is the lowest reaction pressure of phenyl rings reported. However, only two ethynyls of TEB reacted at the most and one left, which resulted in extra stress and disordering in the product. In this work, we investigated the polymerization of 2,6-diethynylpyridine (2,6-DEP) under

Received: January 11, 2024
Revised: April 3, 2024
Accepted: April 9, 2024
Published: April 23, 2024

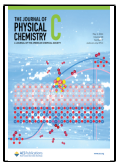

https://doi.org/10.1021/acs.jpcc.4c00211
J. Phys. Chem. C 2024, 128, 7286−7293

high pressure, which avoided the unreacted ethynyl in TEB and is expected to form a perfect carbon-ribbon. However, we found that the ethynyl reacted first at 4−5 GPa, which then drew pyridine ring to react and form a 1-D ordered structure with sp^2/sp^3 hybridization. Our work demonstrates that the PIP of alkynyl in an appropriate stacking can induce the reaction of the aromatic ring at lower pressure by spatial restraints, even if not via the concerted route.

EXPERIMENTAL SECTION

Sample and High-Pressure Generation. 2,6-diethynlpyridine(2,6-DEP) was purchased from TCI. No impurity was detected by powder X-ray diffraction collected on the PANalytical Empyrean diffractometer (Cu K_α radiation; λ = 1.5418 Å). The sample was ground in an agate mortar and loaded into a symmetric diamond anvil cell (DAC) with the anvil culet diameter of 300 um. Type-IIa diamond anvils were used in the IR experiment to avoid the absorption band at 1000−1300 cm^{-1}. T301 stainless steel gaskets were pre-indented to a thickness of 40 μm and holes with a diameter of 160 μm were drilled at the center of the indentations to serve as the sample chamber. The pressure was calibrated by ruby fluorescence,[18] and no pressure medium was used during the experiments.

In Situ Raman and IR Absorption Spectra Experiments. The in situ Raman experiments were performed on a Renishaw Micro-Raman spectroscopy system equipped with a second-harmonic Nd:YAG laser. The wavelength of the laser was 532 nm, and the backscattering geometry was used to collect the Raman data. For the in situ IR spectra, dried KBr powder was pressed into the sample chamber, and then the sample was loaded on top to prevent saturation of the signal. In situ IR without KBr was also carried out for reference. IR experiments were performed on a Bruker VERTEX 70v with a HYPERION 2000 microscope. A Globar instrument was used as a conventional source. The spectra were collected in the transmission mode in the range 600−4000 cm^{-1}, and the resolution was 2 cm^{-1}. The absorption spectrum of the diamond anvil through the same aperture was used as the background.

In Situ X-ray Diffraction Experiments. In situ X-ray diffraction (XRD) data were collected at beamline 4W2 of the Beijing Synchrotron Radiation Facility (BSRF). The wavelength of the incident X-ray was 0.6199 Å. Dioptas[19] was used for data reduction, Jana2006[20] was used for the Le Bail fitting, and TOPAS (version 6)[21] was used for the Rietveld refinement.

Synthesis of Sample (DEP-PE10) Recovered from 10 GPa by Paris-Edinburgh Press. The sample DEP-PE10 was synthesized using a VX3 Paris-Edinburgh (PE) press equipped with stainless-steel gaskets. Single-toroidal tungsten carbide (WC) anvils were used, and the sample volume was 87.1 mm^3. An automatic hydraulic oil syringe pump was used to drive the PE press, and the pressure was estimated according to the Edinburgh group calibration curve.[22] The sample was maintained at 10 GPa for about 24 h and then decompressed to ambient pressure. The rates of the compression and decompression were as follows: 0.05 GPa/min below 2 GPa, 0.04 GPa/min from 2 to 4 GPa, 0.03 GPa/min from 4 to 6 GPa, 0.02 GPa/min from 6 to 8 GPa, 0.01 GPa/min from 8 to 9 GPa, and 0.005 GPa/min from 9 to 10 GPa. The sample DEP-PE10 was obtained after being washed with tetrahydrofuran (THF).

Characterization of DEP-PE10 by X-ray Diffraction, High-Resolution Transmission Electron Microscopy (TEM), and Selected Area Electron Diffraction (SAED). The X-ray diffraction experiment of DEP-PE10 was performed on a PANalytical Empyrean diffractometer (monochromatized Cu K_α radiation; λ = 1.5418 Å), and the data was recorded from 5 to 120°. The high-resolution TEM and SAED patterns were recorded on a JEM-F200 transmission electron microscope under a voltage of 80 kV.

Density Functional Theory Calculation. Density functional theory (DFT) calculations in the Vienna Ab-initio Simulation Package (VASP) code were performed with the projector-augmented plane-wave (PAW) method and the generalized gradient approximation (GGA) in the form of Perdew−Burke−Ernzerhof (PBE) parametrization.[23−28] For optimizations, the kinetic energy cutoff for the plane-wave basis set was 560 eV and Brillouin zone (BZ) was sampled by a k-point mesh with a spacing of $2\pi \times 0.05$ A^{-1}. Then, metadynamics simulation,[29] in which the supercell used contained 16 molecules, 240 atoms, was also implemented in VASP with a 560 eV energy cutoff at 300 K but only the Γ-point was sampled. The simulations were performed using the algorithm of Nosé after the supercell was optimized within the NVT canonical ensemble.[30] Each meta step consisted of 500 molecular dynamics (MD) steps, 0.4 ps in total. The geometry optimization of the Cambridge Sequential Total Energy Package (CASTEP)[31] module in Materials Studio was used to optimize the crystal structures of 2,6-DEP under different pressure and the product models. The optimizations were worked out with the local density approximation (LDA) exchange-correlation functional.[32−34] Generated on the fly (OTFG) norm conserving pseudopotential with a 990 eV energy cutoff and a k-point resolution of $2\pi \times 0.05$ A^{-1} were used in IR and Raman calculations at ambient pressure.

RESULTS AND DISCUSSION

In Situ Raman and IR Spectra under High Pressure. In situ Raman spectra of 2,6-DEP up to 24.1 GPa are shown in Figure 1, and the assignments are displayed in Figure S1. As the pressure increases, all vibrational modes are blue-shifted. At 4.5 GPa, the peaks at 2110, 694, and 652 cm^{-1} were weakened and disappeared. These peaks are attributed to the C≡C stretching vibration and the ≡C−H in-plane and out-of-plane vibration, respectively, and this indicates the reaction of the alkynyl at 4.5 GPa. Upon further compression, the characteristic peaks of the pyridine ring, including those at 1529, 1458, 1247, 1218, and 1134 cm^{-1}, originated from the C−H in-plane and out-of-plane vibrations in ring, were significantly weakened and disappeared at 5.9 GPa, which marked the onset of reaction of the pyridine ring. Above 5.9 GPa, only one peak at 1535 cm^{-1} ascribed to the C═C stretching was obviously observed. The Raman spectra of the sample recovered from 24 GPa showed that the disappeared Raman peaks did not recover, which implies that the reactions of alkynyl and pyridine ring are irreversible.

To avoid the possible effect of laser irradiation, in situ IR spectra of 2,6-DEP were also collected (Figure 2a), and the assignments of the selected IR modes are shown in Figure S2. All the peaks blue-shifted under compression. At 4.9 GPa, the intensities of the ═C−H stretching vibration at 3270 cm^{-1} and the ═C−H in-plane and out-plane vibrations at 738, 701, and 635 cm^{-1} decreased significantly (Figure S3), which is clearly demonstrated by the negative peaks in the difference

https://doi.org/10.1021/acs.jpcc.4c00211
J. Phys. Chem. C 2024, 128, 7286−7293

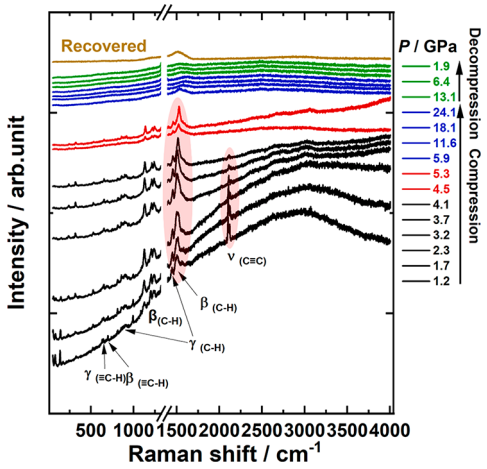

Figure 1. In situ Raman spectra of 2,6-DEP under external pressure. $\beta_{(C-H)}$ and $\beta_{(\equiv C-H)}$ stand for the in-plane bending vibration of C−H bonding in the pyridine ring and ethynyl group, respectively; $\gamma_{(C-H)}$ and $\gamma_{(\equiv C-H)}$ stand for the out-of-plane bending vibration of C−H bonding in the the pyridine ring and ethynyl group, respectively; $\nu_{(C\equiv C)}$ represents the stretching vibration of C≡C in the ethynyl group.

spectrum (Figure 2b) between 4.9 and 4.6 GPa and indicates the alkynyl reacts at 4.6−4.9 GPa. The absorption peaks from the pyridine ring, including the ═C−H stretching vibration peaks at 3072 and 3011 cm^{-1}, C−H in-plane bending vibration peaks at 1587, 1469, 1278, 1213, 1090 cm^{-1}, and out-of-plane bending vibration peaks at 1408 and 822 cm^{-1}, are significantly weakened above 5.7 GPa, indicating the reaction of the pyridine ring (Figure S3). At 8.9 GPa, all sharp characteristic peaks of the alkynyl and pyridine ring disappeared, suggesting that most monomers have already reacted. On the other hand, for the product, the sp^2 C−H stretching peak at 3111 cm^{-1} generated by the reaction of the alkynyl appeared at 7.8 GPa, and the new sp^3 C−H stretching vibration peak was clearly observed during decompression. This is because there is a limited amount of product and pressure suppressed its intensity of the absorption peak.

To clarify the tiny new peaks during compression, we measured in situ IR spectra without KBr (Figure S4). The evolution of IR spectra is consistent with that thinned by KBr, but the pressure of complete reaction was at 11.4 GPa, a little higher than 8.9 GPa. It may be due to the difference of the sample volume and the relaxation of the chemical reaction. The sp^2-C−H stretching vibration peak at 3108 cm^{-1} produced by the reaction of the alkynyl and the sp^3-C−H stretching vibration peak around 2920 cm^{-1} from the reaction of the pyridine ring were observed above 9.1 GPa. These indicate that both the alkynyl and pyridine rings have already reacted. In addition, the sp^3-C−H stretching vibration peak was enhanced with increasing pressure above 11.4 GPa. This is probably because sp^2-C generated by the reaction of the alkynyl transfers into sp^3-C further above 11.4 GPa.

To study the effect of reaction time, the time-dependent in situ IR spectra of 2,6-DEP at 4.6 GPa were collected at room temperature (Figure S5). We analyzed the evolution of IR absorption of the ≡C−H stretching at 3200−3340 cm^{-1} during the reaction process using the Avrami model.[35−38] The fraction of 2,6-DEP reacted (R) as a function of time is described by the following relationship:

$$R(t) = \frac{I(0) - I(t)}{I(0)} = R_{\infty}[1 - e^{[-k(t-t_0)^n]}]$$

where R_∞ is defined as $(I(0) - I(\infty))/I(0)$ and represents a fitting parameter together with the reaction onset time (t_0), the

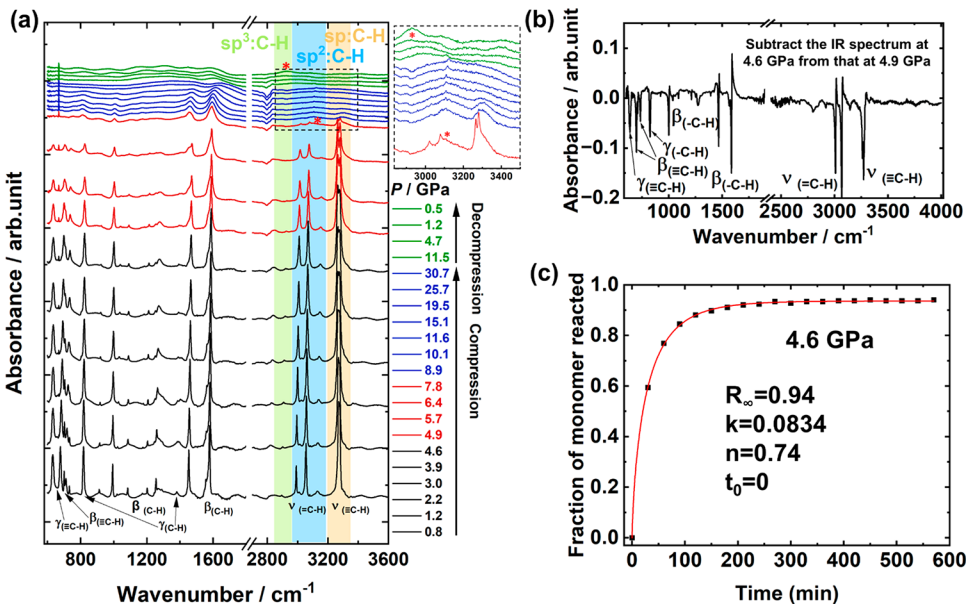

Figure 2. (a) In situ IR spectra of 2,6-DEP thinned with dry KBr powder. (b) Difference spectrum obtained by subtracting the IR absorption spectrum at 4.6 GPa from that at 4.9 GPa. The sharp negative peaks are related to the monomer, whose absorption decreases between the two spectra. (c) Results of fitting the kinetic evolution of samples performed at room temperature and 4.6 GPa. The degree of sample reaction $R(t)$ determined by the absorption peak of the alkynyl band is plotted as a function of time. Fitting parameters are listed in the inset. $\beta_{(C-H)}$ and $\beta_{(\equiv C-H)}$ stand for the in-plane bending vibration of C−H bonding in the pyridine ring and ethynyl group, respectively; $\gamma_{(C-H)}$ and $\gamma_{(\equiv C-H)}$ stand for the out-of-plane bending vibration of C−H bonding in the pyridine ring and ethynyl group, respectively; $\nu_{(=C-H)}$ and $\nu_{(\equiv C-H)}$ represent the C−H stretching vibration of ═C−H group in the pyridine ring and ≡C−H in the ethynyl group. The asterisks represent the appearance of new peaks.

https://doi.org/10.1021/acs.jpcc.4c00211
J. Phys. Chem. C 2024, 128, 7286−7293

rate constant ($k^{1/n}$), and the growth process dimension parameter (n). The sample grows in one dimension if the growth process dimension parameter n is smaller than 1. The plot of fitting is shown in Figure 2c. The result shows that n is smaller than 1, thereby indicating one-dimensional growth of the product at 4.6 GPa. The reaction of 2,6-DEP at 4.6 GPa approached chemical equilibrium after 200 min.

In Situ XRD under High Pressure. 2,6-DEP crystal is monoclinic (space group *Cm*, a = 6.19 Å, b = 17.56 Å, c = 4.05 Å, β = 125.38°, and V = 358.47 Å^3) at atmospheric pressure, and the molecules are parallelly stacked along the c-axis (Figure 3a; the Rietveld refinement plot and atomic coordinates are shown in Figure S6 and Table S1, respectively). To understand the structure evolution of 2,6-DEP under high pressure, we performed in situ synchrotron XRD up to 20.6 GPa, and the results are shown in Figure 3b. From 0.7 to 5.4 GPa, 2,6-DEP maintains the monoclinic lattice, and all the diffractions were broadened and shifted to high angles. The lattice parameters of 2,6-DEP from 0.1 to 5.4 GPa were obtained by Rietveld refinement. As shown in Figure 4a, the lattice parameters a, b and c all decrease gradually with increasing pressure and the compression ratio along the c-axes (12.8%) is greater than that along the a (2.9%) and b-axis (7.1%). This is because the parallel $\pi\cdots\pi$ stacking of pyridine rings is along the c-axis, making it easier to be compressed. The P-V curve of 2,6-DEP up to 5.4 GPa was then fitted with the third-order Birch–Murnaghan equation of state with B_1 fixed at 4 (Figure 4b). The final fitting results are V_0 = 357 ± 7 Å^3 and B_0 = 13 ± 2 GPa. At 6.9 GPa, two new peaks appear at 4.7° (d = 7.5 Å) and 7.6° (d = 4.7 Å), respectively, close to the 020 and 110 peaks, which are attributed to the product according to the spectroscopic result. With increasing pressure, the diffraction peaks of 2,6-DEP disappeared. Above 8.5 GPa, only the two new peaks are visible at 7.5 and 4.7 Å, respectively, and there is no more significant change up to 20.6 GPa and after decompression to atmospheric pressure. The final recovered sample showed two diffraction peaks at 2θ = 4.7° and 7.4° (d = 7.5 and 4.8 Å), demonstrating an ordered product.

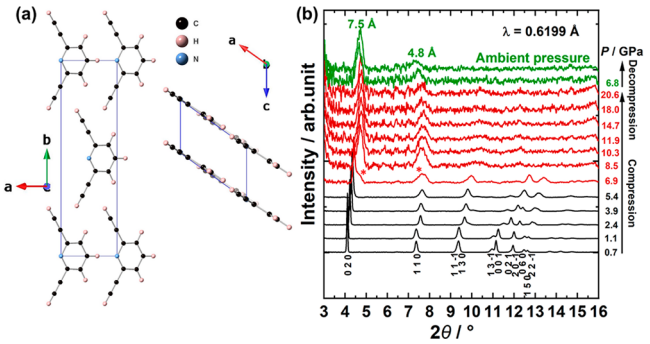

Figure 3. (a) Crystal structure of 2,6-DEP at atmospheric pressure. (b) In situ XRD patterns of 2,6-DEP under a high pressure. The asterisks stand for the appearance of new peaks.

The crystal structures of 2,6-DEP under different pressure before reaction were determined by Rietveld refinement and subsequent optimizations by density functional theory (DFT) calculation, with the lattice parameters fixed at the experimental values (the Rietveld refinement plots and atomic coordinates of 2,6-DEP at 0.7 and 3.9 GPa are shown in Figure S7, Table S2 and Table S3, respectively). The refinement result and crystal structure at 5.4 GPa (space group *Cm*, a = 6.01 Å, b = 16.31 Å, c = 3.53 Å, β = 126.14°) are shown in Figure 4c and d (the atomic coordinates are shown in Table S4). The 2,6-DEP molecules are still stacked along the c-axis at 5.4 GPa. The nearest C···C/C···N distances between the pyridine ring, between the alkynyl and the pyridine ring, and between the alkynyl groups are $d_{C5\cdots N''}$ = 2.90 Å, $d_{C2\cdots 4'}$ = 3.20 Å, and $d_{C1\cdots C2'}$ = 3.35 Å, respectively, with the distance ($d_{C1\cdots C2'}$) between the alkynyl decreasing the fastest (Figure S8). In previous studies, the critical PIP distance of alkyne is 2.9–3.1 Å,[11,12,39,40] while the critical distance for the polymerization of propargyl group in 1-propargyl-4-amino-3,5-dinitro-pyrazole reaches 3.3 Å.[41]

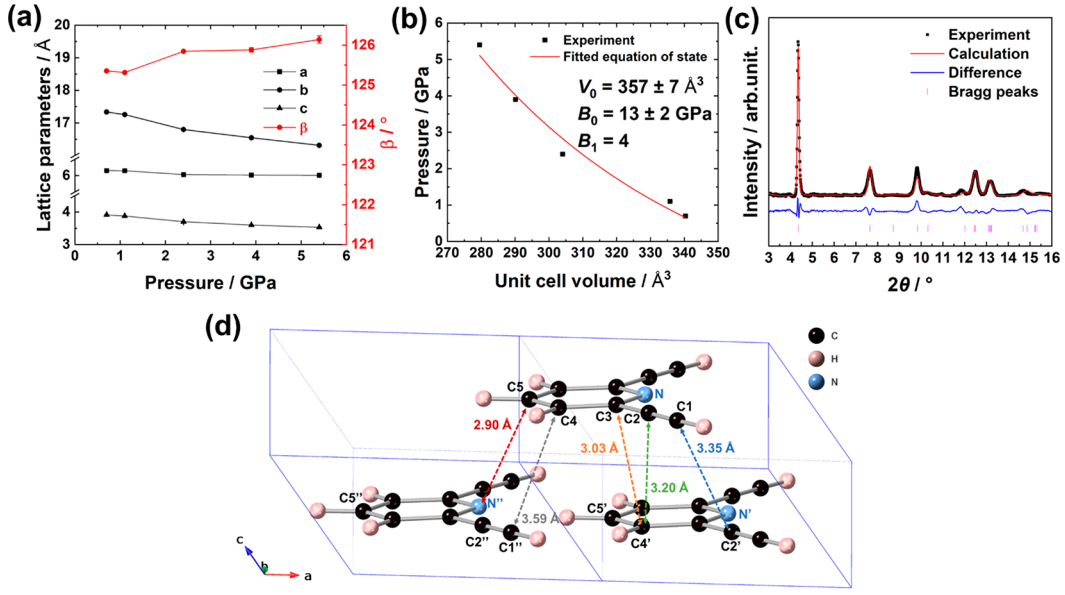

Figure 4. (a) Evolution of the lattice parameters of 2,6-DEP in the range of 0.1–5.4 GPa. The error bars are smaller than the symbol size. (b) P–V relations for 2,6-DEP fitted with the third-order Birch–Murnaghan equation of state with V_0 = 357 ± 7 Å^3, B_0 = 13 ± 2 GPa and B_1 = 4. The error bars are smaller than the symbol size. (c) Rietveld refinement plot of 2,6-DEP at 5.4 GPa. (d) Crystal structure of 2,6-DEP at 5.4 GPa and the C5, N, N', C5', N" and C5" are on the mirror plane.

https://doi.org/10.1021/acs.jpcc.4c00211
J. Phys. Chem. C 2024, 128, 7286–7293

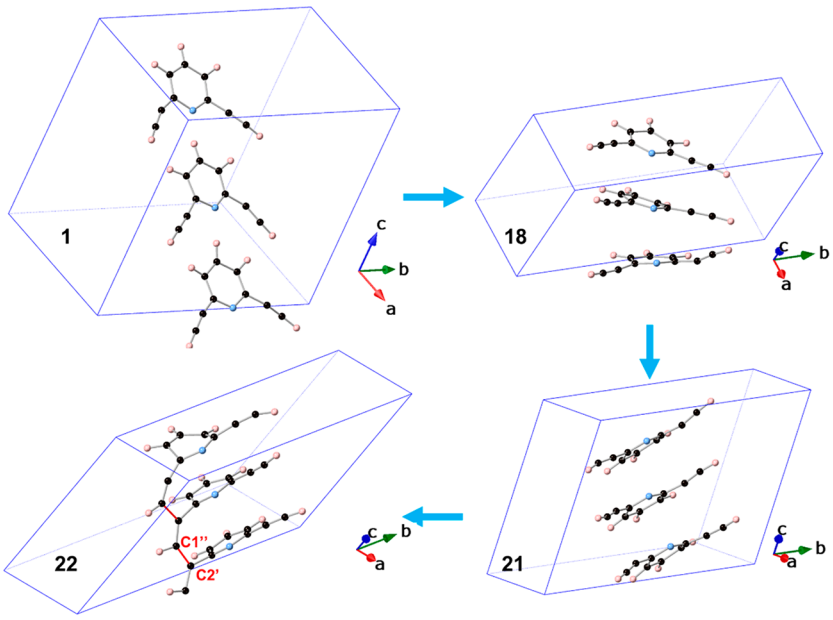

Figure 5. PIP process of 2,6-DEP at 6 GPa, simulated by meta-dynamics. The red bonds were formed among the alkynyls.

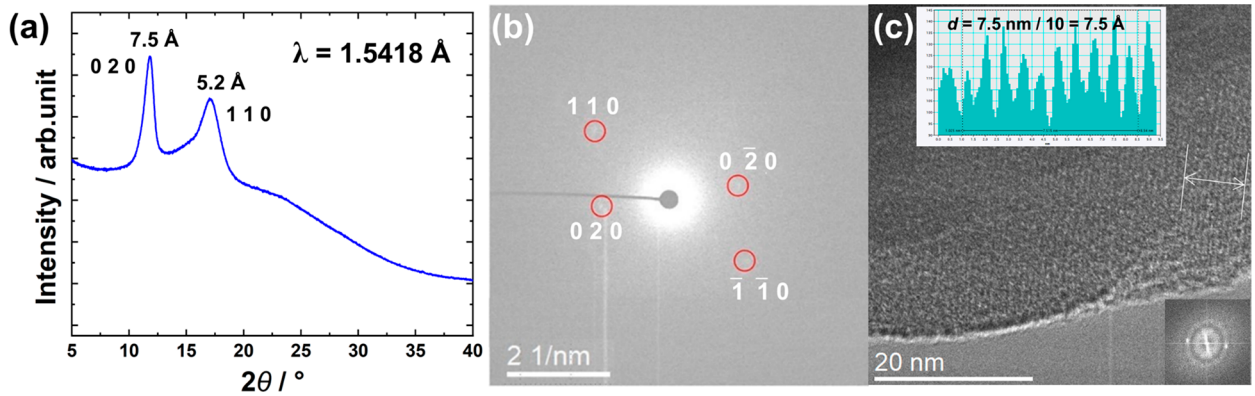

Figure 6. (a) XRD diffraction pattern of DEP-PE10. (b) Selected area electron diffraction results of DEP-PE10. (c) High-resolution electron diffraction results of DEP-PE10, and the inset shows the Fourier transform and line profile.

The critical PIP distance of aromatics is 2.8 Å[8,42] and the critical distance for the concerted reaction of alkynes and aromatics is 3.2−3.4 Å.[16,17] Therefore, if only the critical distances are considered, both the independent and concerted reaction of the alkynyl and the pyridine ring are possible, and we cannot exclude any pathway. However, considering the spectra results, we believe that the alkynyl undergoes polymerization first.

Meta-dynamics Calculation. In order to better describe the PIP process of 2,6-DEP, we expanded the unit cell of 2,6-DEP at ambient pressure in eq 1. The supercell consisted of 16 molecules and was optimized at 6 GPa. Then meta-dynamics calculation (MD) was performed to simulate the PIP process at 300 K.

$$\begin{bmatrix} a' \\ b' \\ c' \end{bmatrix} = \begin{bmatrix} 2 & 0 & 1 \\ 0 & 1 & 0 \\ 0 & 0 & 4 \end{bmatrix} \begin{bmatrix} a \\ b \\ c \end{bmatrix} \quad (1)$$

As shown in Figure 5, the reaction occurred at step 22 of the MD and the reaction starts between the alkynyl groups of the parallelly stacked molecules. The carbon atoms C1"−C2' bonded along the $a-c$ direction (marked by red bonds). Based on the MD results, we found that the bonding of alkynyl significantly reduces the distance between the alkynyl and the pyridine ring and leads to easier further bonding, which will result in a one-dimensional chain structure. It should be noted that this structure shown in Figure 5 is not the final structure, and the polymerization reaction will continue to occur on this basis.

Polymerization Product of 2,6-DEP. To understand the structure of polymerization product, we synthesized the sample (DEP-PE10) with a Paris-Edinburgh (PE) press at 10 GPa and collected the XRD data as shown in Figure 6a. The results show clear diffraction peaks at 2θ = 11.8° and 17.1°, corresponding to d = 7.5 and 5.2 Å, respectively, consistent with the in situ data and demonstrating an obvious ordering. This ordering was also observed in the selected area electron diffraction, as shown in Figure 6b. The peaks in the 2D ordering pattern were indexed as 020 (d_{020} = 7.5 Å) and 110 (d_{110} = 5.2 Å), respectively. Under high-resolution TEM, the product shows a one-dimensional carbon chain structure, and the distinct lattice fringes have a d-spacing of about 7.5 Å (Figure 6c).

https://doi.org/10.1021/acs.jpcc.4c00211
J. Phys. Chem. C 2024, 128, 7286−7293

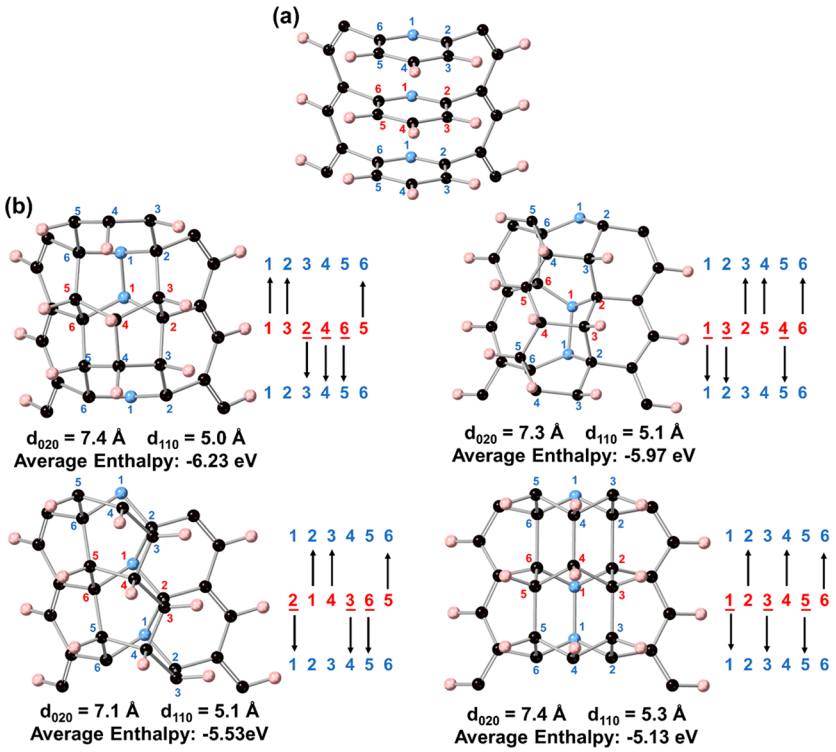

Figure 7. Structure models of the product of 2,6-DEP. (a) Structure model after alkynyl polymerization. (b) Possible structure models of the final product and the relative values of the average enthalpy per C_9H_5N of the models compared to the raw material.

Considering the above results, we constructed and optimized the structure models of the product based on the crystal structure at 5.4 GPa. First, the alkynyl of adjacent molecules in the $\pi-\pi$ stacking direction polymerized to form *trans*-polyethylene structure and the pyridine ring was still stacked in parallel (Figure 7a). Then, based on this structure, we constructed four product structures (Figure 7b) with the degree of saturation 6 (the number of saturated C/N atoms per pyridine unit) by analyzing the possible bonding pathways between pyridine rings and optimized at ambient pressure. The polymer structures of pyridine unit include tube (3,0) (123456), polymer I (132465), polytwistane (214365), and [4 + 2] cycloaddition product followed by a "zipper" reaction (132546). The average energies of the four structures are similar and the simulated *d*-spacings of the product model with tube (3,0) structure fit the experimental data best; however, it is still hard to exclude any models based on the current investigation, and the structure of the product may be a mixture of the above or a disordered one.

Unlike the relatively independent reactions of the alkynyl and benzene rings of PA, DEB, and DPhA, the PIP of alkynyl of 2,6-DEP can induce the reaction of the aromatic ring. In contrast to the PIP of DPB and TEB, there is no evidence of concerted reaction between the alkynyl and the pyridine ring of 2,6-DEP. The reaction pressure of the pyridine ring decreased due to the spatial restraints caused by the polymerization of alkynyl. Compared with TEB, the absence of the third alkynyl changes the arrangement of the molecules and induces a reaction different from that of TEB. Compared with pyridine, the alkynyl in 2,6-DEP leads to parallel stacking of the pyridine ring, which facilitates the PIP. This proves that PIP is closely related to the crystal structure of the reactant. The functional group positions and relative orientations of molecules all affect the reaction of molecules under high pressure.

CONCLUSIONS

In summary, we obtained ordered PIP products of aromatics at lower reaction pressures by introducing the meta-alkynyls. We investigated the high-pressure structural evolution and polymerization mechanism of 2,6-DEP, and found that PIP of alkynyl can reduce the reaction pressure of the pyridine ring by spatial restraints, even if the reactions of the alkynyl and pyridine ring are not concerted. Our study broadens the route for the design and synthesis of a carbon framework at relatively low pressure and provides an important reference for the large-scale preparation of ordered 1-D carbon materials.

ASSOCIATED CONTENT

Supporting Information

The Supporting Information is available free of charge at https://pubs.acs.org/doi/10.1021/acs.jpcc.4c00211.

Assignments of Raman modes of 2,6-DEP at ambient pressure; assignments of IR modes of 2,6-DEP at ambient pressure; the projection of high pressure in situ IR spectra of 2,6-DEP thinned with dry KBr powder; in situ IR spectra of 2,6-DEP without KBr; projection of IR spectra of 2,6-DEP at room temperature and 4.6 GPa with time; Rietveld refinement plot of 2,6-DEP at atmospheric pressure; atomic coordinates of 2,6-DEP at atmospheric pressure; Rietveld refinement plots of 2,6-DEP at 0.7 and 3.9 GPa; atomic coordinates of 2,6-DEP at 0.7 GPa, 3.9 and 5.4 GPa; change of special atom distances between adjacent molecules with pressure (PDF)

https://doi.org/10.1021/acs.jpcc.4c00211
J. Phys. Chem. C 2024, 128, 7286−7293

AUTHOR INFORMATION

Corresponding Authors

Kuo Li − *Center for High Pressure Science and Technology Advanced Research, Beijing 100193, China;* orcid.org/0000-0002-4859-6099; Email: likuo@hpstar.ac.cn

Haiyan Zheng − *Center for High Pressure Science and Technology Advanced Research, Beijing 100193, China;* orcid.org/0000-0002-4727-5912; Email: zhenghy@hpstar.ac.cn

Authors

Yunfan Fei − *Center for High Pressure Science and Technology Advanced Research, Beijing 100193, China*

Yapei Li − *Center for High Pressure Science and Technology Advanced Research, Beijing 100193, China;* Present Address: Institute of Physics, Chinese Academy of Sciences, Beijing 100190, P. R. China

Puyi Lang − *Center for High Pressure Science and Technology Advanced Research, Beijing 100193, China*

Xingyu Tang − *Center for High Pressure Science and Technology Advanced Research, Beijing 100193, China*

Peijie Zhang − *Center for High Pressure Science and Technology Advanced Research, Beijing 100193, China;* Present Address: Southern University of Science and Technology, Shenzhen, Guangdong 518055, P. R. China; orcid.org/0000-0001-6355-5482

Guangwei Che − *Center for High Pressure Science and Technology Advanced Research, Beijing 100193, China*

Xiao Dong − *Key Laboratory of Weak-Light Nonlinear Photonics, School of Physics, Nankai University, Tianjin 300071, P. R. China;* orcid.org/0000-0003-4533-1914

Complete contact information is available at: https://pubs.acs.org/10.1021/acs.jpcc.4c00211

Author Contributions

The manuscript was written through contributions of all authors. All authors have given approval to the final version of the manuscript.

Notes

The authors declare no competing financial interest.

ACKNOWLEDGMENTS

This work was supported by the National Key Research and Development Program of China (2019YFA0708502). The authors also acknowledge the support of the National Natural Science Foundation of China (NSFC) (grant nos.: 22022101 and 21875006). This work was carried out with the support of 4W2 beamline at Beijing Synchrotron Radiation Facility and 15U1 beamline at Shanghai Synchrotron Radiation Facility. This study was partially supported by Synergic Extreme Condition User Facility (SECUF).

REFERENCES

(1) Yang, X.; Wang, X.; Wang, Y.; Li, K.; Zheng, H. From Molecules to Carbon Materials—High Pressure Induced Polymerization and Bonding Mechanisms of Unsaturated Compounds. *Crystals* **2019**, *9*, 490.

(2) Fitzgibbons, T. C.; Guthrie, M.; Xu, E.-s.; Crespi, V. H.; Davidowski, S. K.; Cody, G. D.; Alem, N.; Badding, J. V. Benzene-Derived Carbon Nanothreads. *Nat. Mater.* **2015**, *14*, 43−47.

(3) Li, X.; Wang, T.; Duan, P.; Baldini, M.; Huang, H.-T.; Chen, B.; Juhl, S. J.; Koeplinger, D.; Crespi, V. H.; Schmidt-Rohr, K.; et al. Carbon Nitride Nanothread Crystals Derived from Pyridine. *J. Am. Chem. Soc.* **2018**, *140*, 4969−4972.

(4) Huss, S.; Wu, S.; Chen, B.; Wang, T.; Gerthoffer, M. C.; Ryan, D. J.; Smith, S. E.; Crespi, V. H.; Badding, J. V.; Elacqua, E. Scalable Synthesis of Crystalline One-Dimensional Carbon Nanothreads through Modest-Pressure Polymerization of Furan. *ACS Nano* **2021**, *15*, 4134−4143.

(5) Dunning, S. G.; Zhu, L.; Chen, B.; Chariton, S.; Prakapenka, V. B.; Somayazulu, M.; Strobel, T. A. Solid-State Pathway Control Via Reaction-Directing Heteroatoms: Ordered Pyridazine Nanothreads through Selective Cycloaddition. *J. Am. Chem. Soc.* **2022**, *144*, 2073−2078.

(6) Gao, D.; Tang, X.; Xu, J.; Yang, X.; Zhang, P.; Che, G.; Wang, Y.; Chen, Y.; Gao, X.; Dong, X.; et al. Crystalline $C_3N_3H_3$ Tube (3, 0) Nanothreads. *Proc. Natl. Acad. Sci. U. S. A.* **2022**, *119*, No. e2201165119.

(7) Nobrega, M. M.; Teixeira-Neto, E.; Cairns, A. B.; Temperini, M. L.; Bini, R. One-Dimensional Diamondoid Polyaniline-Like Nanothreads from Compressed Crystal Aniline. *Chem. Sci.* **2018**, *9*, 254−260.

(8) Wang, Y.; Dong, X.; Tang, X.; Zheng, H.; Li, K.; Lin, X.; Fang, L.; Sun, G.; Chen, X.; Xie, L.; et al. Pressure-Induced Diels-Alder Reactions in C_6H_6-C_6F_6 Cocrystal Towards Graphane Structure. *Angew. Chem., Int. Ed.* **2019**, *58*, 1468−1473.

(9) Sakashita, M.; Yamawaki, H.; Aoki, K. FT-IR Study of the Solid State Polymerization of Acetylene under Pressure. *J. Phys. Chem.* **1996**, *100*, 9943−9947.

(10) Aoki, K.; Usuba, S.; Yoshida, M.; Kakudate, Y.; Tanaka, K.; Fujiwara, S. Raman Study of the Solid-State Polymerization of Acetylene at High Pressure. *J. Chem. Phys.* **1988**, *89*, 529−534.

(11) Sun, J.; Dong, X.; Wang, Y.; Li, K.; Zheng, H.; Wang, L.; Cody, G. D.; Tulk, C. A.; Molaison, J. J.; Lin, X.; et al. Pressure-Induced Polymerization of Acetylene: Structure-Directed Stereoselectivity and a Possible Route to Graphane. *Angew. Chem., Int. Ed.* **2017**, *129*, 6653−6657.

(12) Tang, X.; Dong, X.; Zhang, C.; Li, K.; Zheng, H.; Mao, H.-k. Triggering Dynamics of Acetylene Topochemical Polymerization. *Matter Radiat. at Extremes* **2023**, *8*, 058402.

(13) Santoro, M.; Ciabini, L.; Bini, R.; Schettino, V. High-Pressure Polymerization of Phenylacetylene and of the Benzene and Acetylene Moieties. *J. Raman Spectrosc.* **2003**, *34*, 557−566.

(14) Tang, W. S.; Strobel, T. A. Evidence for Functionalized Carbon Nanothreads from π-Stacked, Para-Disubstituted Benzenes. *J. Phys. Chem. C* **2020**, *124*, 25062−25070.

(15) Romi, S.; Fanetti, S.; Alabarse, F. G.; Bini, R.; Santoro, M. High-Pressure Synthesis of 1D Low-Bandgap Polymers Embedded in Diamond-Like Carbon Nanothreads. *Chem. Mater.* **2022**, *34*, 2422−2428.

(16) Zhang, P.; Tang, X.; Wang, Y.; Wang, X.; Gao, D.; Li, Y.; Zheng, H.; Wang, Y.; Wang, X.; Fu, R.; et al. Distance-Selected Topochemical Dehydro-Diels-Alder Reaction of 1, 4-Diphenylbutadiyne toward Crystalline Graphitic Nanoribbons. *J. Am. Chem. Soc.* **2020**, *142*, 17662−17669.

(17) Li, Y.; Tang, X.; Zhang, P.; Wang, Y.; Yang, X.; Wang, X.; Li, K.; Wang, Y.; Wu, N.; Tang, M.; et al. Scalable High-Pressure Synthesis of sp^2-sp^3 Carbon Nanoribbon Via [4 + 2] Polymerization of 1, 3, 5-Triethynylbenzene. *J. Phys. Chem. Lett.* **2021**, *12*, 7140−7145.

(18) Mao, H.; Xu, J.-A.; Bell, P. Calibration of the Ruby Pressure Gauge to 800 kbar under Quasi-Hydrostatic Conditions. *J. Geophys. Res.: Solid Earth* **1986**, *91*, 4673−4676.

(19) Prescher, C.; Prakapenka, V. B. Dioptas: A Program for Reduction of Two-Dimensional X-Ray Diffraction Data and Data Exploration. *High Pressure Res.* **2015**, *35*, 223−230.

(20) Petříček, V.; Dušek, M.; Palatinus, L. Crystallographic Computing System Jana2006: General Features. *Z. Kristallogr.* **2014**, *229*, 345−352.

(21) Coelho, A. A. Topas and Topas-Academic: An Optimization Program Integrating Computer Algebra and Crystallographic Objects Written in C++. *J. Appl. Crystallogr.* **2018**, *51*, 210−218.
(22) Salmon, P. S.; Drewitt, J. W.; Whittaker, D. A.; Zeidler, A.; Wezka, K.; Bull, C. L.; Tucker, M. G.; Wilding, M. C.; Guthrie, M.; Marrocchelli, D. Density-Driven Structural Transformations in Network Forming Glasses: A High-Pressure Neutron Diffraction Study of GeO_2 Glass up to 17.5 GPa. *J. Phys.: Condens. Matter* **2012**, *24*, 415102.
(23) Jones, R. O. Density Functional Theory: Its Origins, Rise to Prominence, and Future. *Rev. Mod. Phys.* **2015**, *87*, 897−923.
(24) Kresse, G.; Hafner, J. Ab Initio Molecular Dynamics for Liquid Metals. *Phys. Rev. B* **1993**, *47*, 558−561.
(25) Kresse, G.; Furthmüller, J. Efficiency of Ab-Initio Total Energy Calculations for Metals and Semiconductors Using a Plane-Wave Basis Set. *Comput. Mater. Sci.* **1996**, *6*, 15−50.
(26) Kresse, G.; Joubert, D. From Ultrasoft Pseudopotentials to the Projector Augmented-Wave Method. *Phys. Rev. B* **1999**, *59*, 1758−1775.
(27) Kresse, G.; Furthmüller, J. Efficient Iterative Schemes for Ab Initio Total-Energy Calculations Using a Plane-Wave Basis Set. *Phys. Rev. B* **1996**, *54*, 11169−11186.
(28) Perdew, J. P.; Burke, K.; Ernzerhof, M. Generalized Gradient Approximation Made Simple. *Phys. Rev. Lett.* **1996**, *77*, 3865−3868.
(29) Barducci, A.; Bonomi, M.; Parrinello, M. Metadynamics. *Wiley Interdiscip. Rev.: Comput. Mol. Sci.* **2011**, *1*, 826−843.
(30) Nosé, S. A Unified Formulation of the Constant Temperature Molecular Dynamics Methods. *J. Chem. Phys.* **1984**, *81*, 511−519.
(31) Clark, S. J.; Segall, M. D.; Pickard, C. J.; Hasnip, P. J.; Probert, M. I.; Refson, K.; Payne, M. C. First Principles Methods Using Castep. *Z. Kristallogr.* **2005**, *220*, 567−570.
(32) Perdew, J. P.; Zunger, A. Self-Interaction Correction to Density-Functional Approximations for Many-Electron Systems. *Phys. Rev. B* **1981**, *23*, 5048−5079.
(33) Blöchl, P. E. Projector Augmented-Wave Method. *Phys. Rev. B* **1994**, *50*, 17953−17979.
(34) Baroni, S.; De Gironcoli, S.; Dal Corso, A.; Giannozzi, P. Phonons and Related Crystal Properties from Density-Functional Perturbation Theory. *Rev. Mod. Phys.* **2001**, *73*, 515−562.
(35) Avrami, M. Kinetics of Phase Change. I General Theory. *J. Chem. Phys.* **1939**, *7*, 1103−1112.
(36) Avrami, M. Kinetics of Phase Change. II Transformation-Time Relations for Random Distribution of Nuclei. *J. Chem. Phys.* **1940**, *8*, 212−224.
(37) Avrami, M. Granulation, Phase Change, and Microstructure Kinetics of Phase Change. III. *J. Chem. Phys.* **1941**, *9*, 177−184.
(38) Hulbert, S. Models for Solid-State Reactions in Powdered Compacts-a Review. *J. Brit Ceram Soc.* **1969**, *6*, 11−20.
(39) Zheng, H.; Wang, L.; Li, K.; Yang, Y.; Wang, Y.; Wu, J.; Dong, X.; Wang, C.-H.; Tulk, C. A.; Molaison, J. J.; et al. Pressure Induced Polymerization of Acetylide Anions in CaC_2 and 10^7 Fold Enhancement of Electrical Conductivity. *Chem. Sci.* **2017**, *8*, 298−304.
(40) Han, J.; Tang, X.; Wang, Y.; Wang, Y.; Han, Y.; Lin, X.; Dong, X.; Lee, H. H.; Zheng, H.; Li, K.; et al. Pressure-Induced Polymerization of Monosodium Acetylide: A Radical Reaction Initiated Topochemically. *J. Phys. Chem. C* **2019**, *123*, 30746−30753.
(41) Qi, G.; Song, S.; Deng, Z.; Huang, D.; Chen, F.; Yan, B.; Gou, H.; Zhang, Q.; Wang, Y. Pressure-Induced Topochemical Polymerization toward Advanced Energetic Materials. *CCS Chem.* **2023**, *5*, 1815−1826.
(42) Ciabini, L.; Santoro, M.; Gorelli, F. A.; Bini, R.; Schettino, V.; Raugei, S. Triggering Dynamics of the High-Pressure Benzene Amorphization. *Nat. Mater.* **2007**, *6*, 39−43.

https://doi.org/10.1021/acs.jpcc.4c00211
J. Phys. Chem. C 2024, 128, 7286−7293